ChemComm

Check for updates

Ru-Coated metal–organic framework-derived Co-based particles embedded in porous N-doped carbon nanocubes as a catalytic cathode for a Li–O₂ battery†

Dongdong Li,‡ Haocheng Qi,‡ Huiming Zhao, Ling Ding, Zhaoxiang Zhang and Ziyang Guo ⓘ *

Co₄N/Co-NC was synthesized through pyrolysis of ZIF-67 and modified with Ru nanoparticles to form Ru-Co₄N/Co-NC. The resulting Ru-Co₄N/Co-NC is used as a cathode for a Li–O₂ battery, which shows good electrochemical performances.

With the rapid consumption of fossil fuels, the pursuit of green energy storage systems has become urgent for modern society.[1] Lithium (Li)-ion batteries, which is considered as the state-of-the-art energy storage component, cannot meet the development demand of the next-generation electric vehicles due to their limited theoretical energy density.[2] Hence, Li–O₂ batteries have attracted worldwide attention due to their super-high energy.[3] However, there are still several critical challenges before applications of Li–O₂ batteries.[4] The major problem for Li–O₂ batteries is derived from the sluggish oxygen reduction/evolution reaction (ORR/OER) kinetics and insulating/insoluble Li₂O₂ on the cathode, which lead to a huge overpotential and inferior cycle life.[5] Hence, designing effective catalysts with superior electronic conductivity and adequate porous structure is crucial for Li–O₂ batteries.

Carbon materials have been widely studied as catalysts for Li–O₂ batteries due to their light mass and abundant pores.[6] However, carbon catalysts usually have poor OER activities and face serious side reactions.[7] Metal-based materials have been considered as suitable alternative cathodes to carbon in Li–O₂ batteries because of their relatively high catalytic activity/stability.[8] However, the metal-based active sites are easily agglomerated during cycling. Metal–organic frameworks (MOFs) have been investigated as effective catalysts since their stable framework and molecular coordination can suppress agglomeration of active sites.[9a,b] Owing to the poor conductivity of these MOFs, they must be mixed with carbon materials which cause serious side reactions in Li–O₂ batteries.[9c] MOFs-derived

materials recently have aroused a great deal of interest since they not only can preserve the main advantages of the original MOFs, but also show enhanced electronic conductivity.[9d] However, the exposed carbon species on the MOF-derived matrices can partially react with electrolyte and even be oxidized in Li–O₂ batteries. On the other hand, it is well known that ruthenium (Ru)-based materials can restrain side reactions induced by carbon species in Li–O₂ batteries.[10] Hence, Ru-based nanocrystal coated MOFs-derived materials will be ideal cathode catalysts for Li–O₂ batteries. Up to now, there is almost no investigation about this topic.

Herein, we designed Co₄N/Co nanoparticles embedded into porous N-doped carbon nanocubes (Co₄N/Co-NC) through pyrolysis of zeolitic-imidazole frameworks (ZIFs), and loaded Ru particles on the Co₄N/Co-NC matrix to form Ru-coated Co₄N/Co-NC (Ru-Co₄N/Co-NC). The porous carbon framework in Ru-Co₄N/Co-NC can facilitate the diffusion of electrons/ions and O₂ and inhibit the agglomeration of Co-based active sites. In addition, the uniformly distributed Co₄N/Co nanoparticles and high surface N content can effectively improve the catalytic activities towards both OER/ORR. Moreover, the Ru-coating layer can obviously alleviate side reactions. Hence, the Ru-Co₄N/Co-NC based Li–O₂ cell shows good performances.

As illustrated in Fig. 1a, cubic ZIF-67 was synthesized through the coordination reaction between cobalt nitrate and 2-methylimidazole and then carbonized to form Co₄N/Co nanoparticles encapsulated into N-doped porous carbon nanocubes (Co₄N/Co-NC). After treatment with RuCl₃, Ru-coated Co₄N/Co-NC (Ru-Co₄N/Co-NC) is finally obtained (see Experimental section for details, ESI†). Field emission scanning and transmission electron microscopy (SEM/TEM) images of Ru-Co₄N/Co-NC were carried out. Fig. 1b and c show that the morphology of Ru-Co₄N/Co-NC is the typical nanocube structure, which is in agreement with those of ZIF-67 and Co₄N/Co-NC (Fig. S1 and S2, ESI†). This phenomenon demonstrates that Ru-coating and calcination do not disrupt the basic structure of ZIF-67. Fig. 1c indicates that there are several Co-based nanoparticles with uniform particle size of ∼30 nm embedded in the carbon

Key Laboratory of Eco-Chemical Engineering, Taishan Scholar Advantage and Characteristic Discipline Team of Eco Chemical Process and Technology, College of Chemistry and Molecular Engineering, Qingdao University of Science and Technology, Qingdao 266042, China. E-mail: zyguo@qust.edu.cn

† Electronic supplementary information (ESI) available. See DOI: 10.1039/c9cc04720d
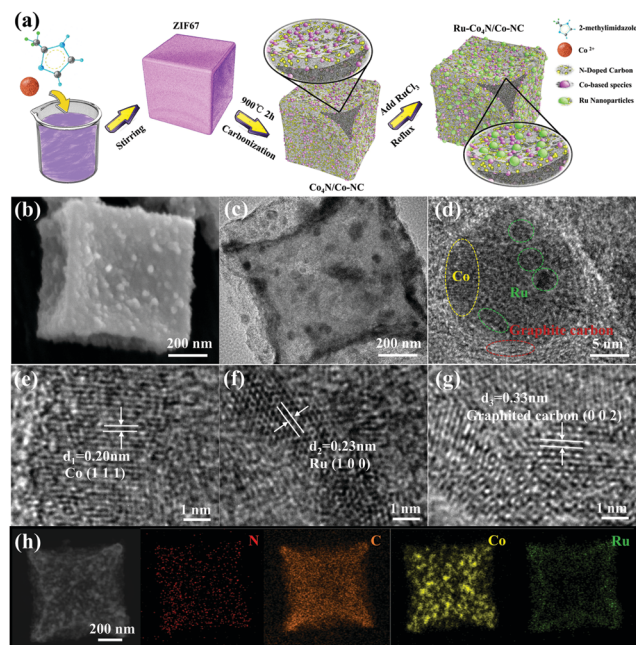‡ Dongdong Li and Haocheng Qi contributed equally to this work.

Fig. 1 (a) Schematic illustration of the synthetic process, (b) SEM and (c)–(g) TEM images of Ru-Co$_4$N/Co-NC; (h) TEM image of Ru-Co$_4$N/Co-NC and the corresponding EDX mapping images.

Fig. 2 XRD patterns (a) and full XPS spectra (b) of Ru-Co$_4$N/Co-NC and Co$_4$N/Co-NC; high-resolution XPS spectra: (c) Co 2p$_{3/2}$ and (d) C 1s and Ru 3d; (e) N$_2$ adsorption/desorption isotherms and (f) pore-size distribution of Ru-Co$_4$N/Co-NC.

framework. In addition, it can be further found from enlarged TEM images in Fig. 1d–g that there are three different kinds of lattice distances (d): d_1 = 0.20 nm, d_2 = 0.23 nm and d_3 = 0.33 nm, which are assigned to the (111) layer of metallic Co, (100) plane of metallic Ru and (002) layer of graphitic carbon, respectively. Moreover, energy-dispersive X-ray (EDX) mapping investigation of Ru-Co$_4$N/Co-NC was also carried out (Fig. 1h). As shown in Fig. 1h, N, C, Co and Ru elements were evenly distributed in the framework, further indicating the successful introduction of Ru species in Ru-Co$_4$N/Co-NC.

X-Ray diffraction (XRD) patterns of Ru-Co$_4$N/Co-NC and its precursor were investigated. The XRD pattern of the initial precursor is almost identical to the standard diffraction peak pattern of ZIF-67 (Fig. S3, ESI†) indicating the successful preparation of ZIF-67. Fig. 2a shows that Co$_4$N/Co-NC has main peaks at around 44.2 and 51.6°, which are assigned to Co and Co$_4$N species.[11,12] In the XRD pattern of Ru-Co$_4$N/Co-NC, the peaks attributed to Co and Co$_4$N phases show an obvious decrease and new peaks at around 38.4, 44.0, 58.3, and 69.4° ascribed to metallic Ru are formed.[12b] These results suggest that Ru nanoparticles are uniformly coated on the surface of Ru-Co$_4$N/Co-NC. Raman spectra of both Co$_4$N/Co-NC and Ru-Co$_4$N/Co-NC present typical G- and D-bands (Fig. S4, ESI†), confirming the existence of graphitized carbon after calcination. To further analyze the composition of Co$_4$N/Co-NC and Ru-Co$_4$N/Co-NC, X-ray photoelectron spectroscopy (XPS) was also carried out. Ru, Co, N, O and C elements are present in Ru-Co$_4$N/Co-NC, but only Co, N, O and C elements occur in Co$_4$N/Co-NC (Fig. 2b), further indicating the successful introduction of Ru in Ru-Co$_4$N/Co-NC. In the high-resolution Co 2p XPS spectra of Ru-Co$_4$N/Co-NC (Fig. 2c), there are three assumed types of
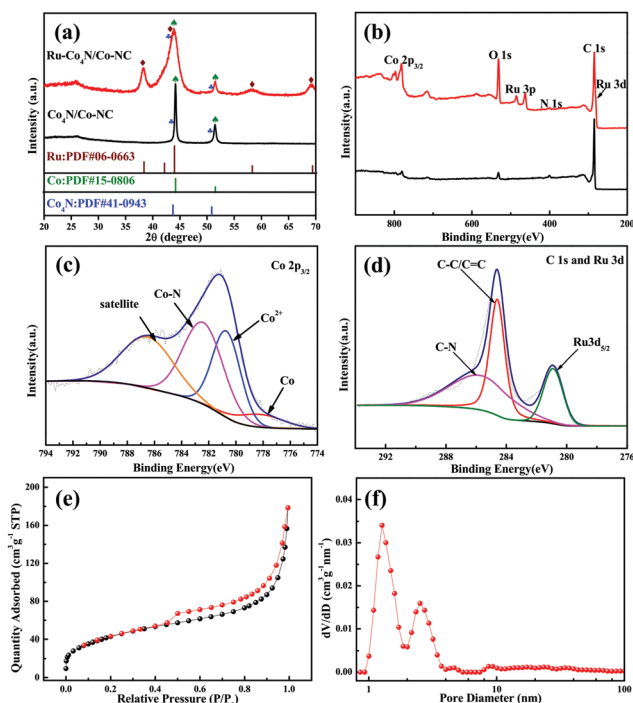
Co species: metallic Co ($\sim$778.1 eV), Co^{2+} ($\sim$780.7 eV), Co–N ($\sim$782.6 eV) and satellite ($\sim$786.5 eV), respectively.[12] Moreover, the surface content of Co–N, which enhances OER activity, is high in Ru-Co$_4$N/Co-NC. The high-resolution C 1s/Ru 3d XPS spectra shown in Fig. 2d indicate that there are three sub-peaks in Ru-Co$_4$N/Co-NC: C–C (284.6 eV), C–N (285.5 eV) and Ru 3d$_{5/2}$ (280.9 eV), respectively.[11,12d] As shown in Fig. 2e, N$_2$ adsorption/ desorption plots of Ru-Co$_4$N/Co-NC shows an obvious increase below a relative pressure of 0.05 and a pronounced hysteresis at the pressure range of 0.4–0.9, suggesting the co-existence of micro/mesopores in Ru-Co$_4$N/Co-NC. Furthermore, the pore-size distribution data show that micropores ($\sim$1.3 nm) and mesopores ($\sim$2.5 nm) are the main pores in Ru-Co$_4$N/Co-NC (Fig. 2f), which is different from that of the pristine Co$_4$N/Co-NC (Fig. S5, ESI†). This result indicates that the Ru coating layer can regulate the porous nature of Co/Co$_4$N-NC to some extent. Moreover, the Brunauer–Emmett–Teller (BET) surface areas of Co$_4$N/Co-NC and Ru-Co$_4$N/Co-NC are 338 and 142 m^2 g^{-1}, respectively, suggesting that the Ru-coating layer slightly decreases the surface area of the pristine Co$_4$N/Co-NC.

Fig. 3a shows voltage curves of Ru-Co$_4$N/Co-NC, Co$_4$N/Co-NC and KB based Li–O$_2$ batteries at 100 mA g^{-1} between 2.0 and 4.3 V, respectively. As shown in Fig. 3a, the discharge capacities of Ru-Co$_4$N/Co-NC and Co$_4$N/Co-NC electrodes can reach 14 449 and 7676 mA h g^{-1}, while KB cathode can only exhibit 4193 mA h g^{-1}. Fig. 3b shows that the Ru-Co$_4$N/Co-NC cathode still displays higher discharge capacities than Co$_4$N/Co-NC and KB electrodes even at higher current densities of 200 and
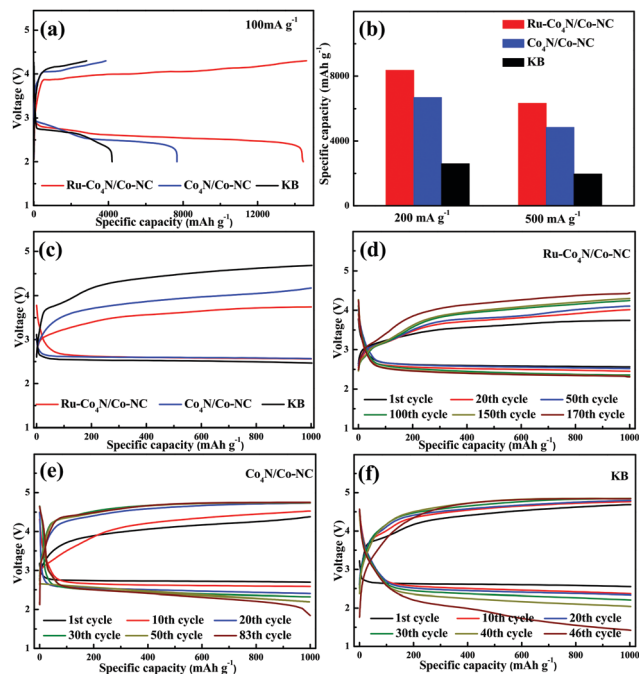
Fig. 3 (a) Voltage profiles at 100 mA g^{-1} between 2.0 and 4.3 V, (b) discharge capacities at different densities, (c) discharge/charge curves under the first cycle and (d)–(f) cycle performances at 500 mA g^{-1} with limited capacity of 1000 mA h g^{-1} for Ru-Co$_4$N/Co-NC, Co$_4$N/Co-NC and KB electrodes, respectively.

500 mA g^{-1}, demonstrating the superior rate performance of the Ru-Co$_4$N/Co-NC cathode. Voltage profiles of Ru-Co$_4$N/Co-NC, Co$_4$N/Co-NC and KB cathodes were also studied at 500 mA g^{-1} with a limited capacity of 1000 mA h g^{-1} (Fig. 3c). It can be observed from Fig. 3c that the overpotential of the Ru-Co$_4$N/Co-NC electrode is obviously lower than those of Co$_4$N/Co-NC and KB cathodes, confirming that synergy of the Ru coated layer and Co-based nanoparticles can reduce the decomposition voltage of discharge products. Cycle performances of Ru-Co$_4$N/Co-NC, Co$_4$N/Co-NC and KB cathodes were also investigated under the restricted capacity measurements (Fig. 3d–f). The Ru-Co$_4$N/Co-NC cathode can be stably operated over 170 cycles (Fig. 3d), which is comparable to most recently reported state-of-the-art cathode catalysts (Table S1, ESI†). In addition, it should be noted that the Co$_4$N/Co-NC cathode can also steadily run for 80 cycles, but shows an obvious voltage drop below 2.0 V after 83 cycles (Fig. 3e). Moreover, Fig. 3f shows that the voltages of the KB cathode at the end of discharge rapidly decline to < 2.0 V after 46 cycles. Moreover, Fig. S6 (ESI†) shows that the electrochemical performances of the Ru-KB cathode (preparation of Ru-KB cathode is given in ESI†) are also inferior compared with the Ru-Co$_4$N/Co-NC electrode, which further demonstrates that the unique combination of the Ru coating layer and Co-based NC framework can enhance the performance of Li–O$_2$ batteries. The superior performance of the Ru-Co$_4$N/Co-NC cathode can be ascribed to the uniform Ru coating layer, highly distributed Co-based nanoparticles, plentiful pores and N-doped carbon framework in Ru-Co$_4$N/Co-NC.

To clarify the architecture effect of Ru-Co$_4$N/Co-NC on the performance of Li–O$_2$ batteries, the surface morphologies of Ru-Co$_4$N/Co-NC electrodes at different discharge/charge stages were investigated by SEM (Fig. S7, ESI†). There are many cubic Ru-Co$_4$N/Co-NCs in the pristine cathode. After discharge, many Li$_2$O$_2$ particles with a size of ∼50 nm are coated around Ru-Co$_4$N/Co-NC (Fig. S7, ESI†). After recharging, such particle-sized products completely vanish and cubic Ru-Co$_4$N/Co-NCs re-emerge, indicating the electrochemical stability of Ru-Co$_4$N/Co-NC. To further understand the composition of products on Ru-Co$_4$N/Co-NC cathodes over cycling, *ex situ* XRD and Fourier transform-infrared spectroscopy (FT-IR) measurements were also conducted (Fig. 4a and b). Compared with the XRD pattern of the initial Ru-Co$_4$N/Co-NC cathode, several diffraction peaks indexed to Li$_2$O$_2$ are generated on the discharged Ru-Co$_4$N/Co-NC electrode. At the end of recharge, these characteristic peaks related to Li$_2$O$_2$ have disappeared again on the XRD pattern of the Ru-Co$_4$N/Co-NC cathode (Fig. 4a). In addition, FT-IR spectra also indicate that Li$_2$O$_2$ is formed during the discharge process and then decomposed after recharging (Fig. 4b). These results further confirm the reversibility of the Ru-Co$_4$N/Co-NC electrode. However, it should be noted that there is a small amount of amorphous side products (*e.g.* Li$_2$CO$_3$) formed on the discharged Ru-Co$_4$N/Co-NC cathode. In order to further reveal reactions on the Ru-Co$_4$N/Co-NC cathode, *in situ* differential electrochemical mass spectrometry (DEMS) was also conducted to analyze gas consumption/evolution over discharging and recharging processes (Fig. S8, ESI†). For comparison, KB cathode was also tested by *in situ* DEMS under the same conditions (Fig. S9, ESI†). It can be found from Fig. 4c and Fig. S9a (ESI†) that O$_2$ is consumed during discharge at both Ru-Co$_4$N/Co-NC and KB cathodes. On recharging, the charge voltage of the Ru-Co$_4$N/Co-NC electrode is smaller compared with the KB cathode, further suggesting superior OER catalytic activity of Ru-Co$_4$N/Co-NC in Li–O$_2$ cells. Although both O$_2$ and CO$_2$ are released at Ru-Co$_4$N/Co-NC and KB
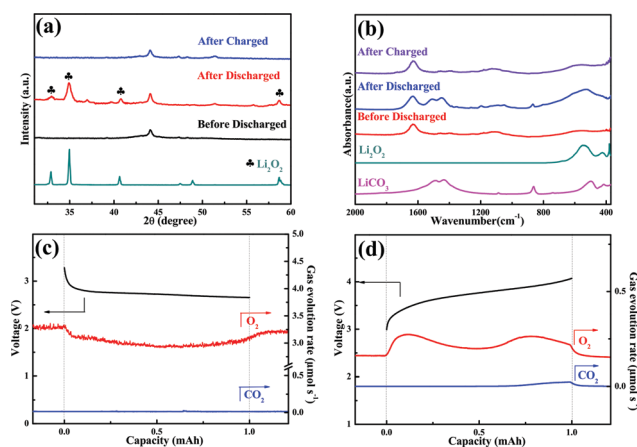

Fig. 4 (a) XRD patterns and (b) IR spectra of Ru-Co$_4$N/Co-NC at different states. Gas evolution and corresponding voltage curves of the Ru-Co$_4$N/Co-NC cathode at 0.5 mA with limited capacity of 1.0 mA h; (c) discharging and (d) charging.

cathodes during charging (Fig. 4d and Fig. S9b, ESI†), the quantity of evolved CO_2 for the Ru-Co_4N/Co-NC electrode is obviously lower than that for the KB cathode. These above results further demonstrate that Ru-Co_4N/Co-NC can effectively reduce side reactions and improve the reversibility of Li–O_2 batteries.

In summary, Co_4N/Co-NC was synthesized through pyrolysis of ZIF-67 and further coated with Ru nanoparticles to form Ru-Co_4N/Co-NC. The Ru coating layer coupled with uniform Co_4N/Co nanoparticles can effectively promote decomposition of discharge products. N-doped porous carbon matrix provides enough channels to transfer O_2/ion for reactions in Li–O_2 batteries. Hence, Ru-Co_4N/Co-NC based Li–O_2 battery shows super-high capacity, low charge overpotential and long cycling life. A series of *ex situ* SEM, FT-IR, PXRD and *in situ* DEMS investigations were conducted to confirm that Ru-Co_4N/Co-NC is stable and enhances the reversibility of Li–O_2 cells. However, slight electrolyte decomposition still exists in Ru-Co_4N/Co-NC based Li–O_2 batteries. Hence, developing highly active carbon-free cathodes coupled with stable electrolytes should be the next logical step for Li–O_2 batteries.

Conflicts of interest

There are no conflicts to declare.

Notes and references

1 (a) S. Chu, Y. Cui and N. Liu, *Nat. Mater.*, 2017, **16**, 16; (b) J. Qi, X. Y. Lai, J. Y. Wang, H. J. Tang, H. Ren, Y. Yang, Q. Jin, L. J. Zhang, R. B. Yu, G. H. Ma, Z. G. Su, H. J. Zhao and D. Wang, *Chem. Soc. Rev.*, 2015, **44**, 6749; (c) B. Liu, Y. L. Sun, L. Liu, S. Xu and X. B. Yan, *Adv. Funct. Mater.*, 2018, **28**, 1704973; (d) X. P. Han, X. P. Li, J. White, C. Zhong, Y. D. Deng and T. Y. Ma, *Adv. Energy Mater.*, 2018, **8**, 1801396.
2 (a) J. Lu, L. Li, J. B. Park, Y. K. Sun, F. Wu and K. Amine, *Chem. Rev.*, 2014, **114**, 5611; (b) J. Y. Wang, H. J. Tang, L. J. Zhang, H. Ren, R. B. Yu, Q. Jin, J. Qi, D. Mao, M. Yang, Y. Wang, P. Liu, Y. Zhang, Y. R. Wen, L. Gu, G. H. Ma, Z. G. Su, Z. Y. Tang, H. J. Zhao and D. Wang, *Nat. Energy*, 2016, **1**, 16050; (c) Q. Zhao, N. Katyal,

I. D. Seymour, G. Henkelman and T. Y. Ma, *Angew. Chem., Int. Ed.*, 2019, DOI: 10.1002/anie.201907477.
3 (a) X. X. Shen, S. S. Zhang, Y. P. Wu and Y. H. Chen, *ChemSusChem*, 2019, **12**, 104; (b) F. J. Li and J. Chen, *Adv. Energy Mater.*, 2017, **7**, 1602934.
4 (a) J. J. Xu and X. B. Zhang, *Nat. Energy*, 2017, **2**, 17133; (b) N. Feng, P. He and H. S. Zhou, *Adv. Energy Mater.*, 2016, **6**, 1502303.
5 (a) Y. T. Zhang, L. Wang, X. Z. Zhang, L. M. Guo, Y. Wang and Z. Q. Peng, *Adv. Mater.*, 2018, **30**, 1705571; (b) M. D. Radin and D. J. Siegel, *Energy Environ. Sci.*, 2013, **6**, 2370.
6 (a) H. D. Lim, K. Y. Park, H. Song, E. Y. Jang, H. Gwon, J. Kim, Y. H. Kim, M. D. Lima, R. O. Robles, X. Lepró, R. H. Baughman and K. Kang, *Adv. Mater.*, 2013, **25**, 1348; (b) B. Sun, S. Q. Chren, H. Liu and G. X. Wang, *Adv. Funct. Mater.*, 2015, **25**, 4436; (c) G. Huang, J. H. Han, C. C. Yang, Z. Q. Wang, T. Fujita, A. Hirata and M. W. Chen, *NPG Asia Mater.*, 2018, **10**, 1037.
7 (a) M. M. Ottakam Thotiyl, S. A. Freunberger, Z. Peng and P. G. Bruce, *J. Am. Chem. Soc.*, 2013, **135**, 494; (b) B. D. McCloskey, A. Speidel, R. Scheffler, D. C. Miller, V. Viswanathan, J. S. Hummelshøj, J. K. Nørskov and A. C. Luntz, *J. Phys. Chem. Lett.*, 2012, **3**, 997.
8 (a) J. D. Liu, Y. Y. Zhao, X. Li, C. G. Wang, Y. P. Zeng, G. H. Yue and Q. Chen, *Nano-Micro Lett.*, 2018, **10**, 22; (b) X. Z. Ren, M. J. Huang, S. Luo, Y. L. Li, L. B. Deng, H. W. Mi, L. N. Sun and P. X. Zhang, *J. Mater. Chem. A*, 2018, **6**, 10856.
9 (a) X. H. Zhang, P. P. Dong and M. K. Song, *Batteries & Supercaps*, 2019, **2**, 1; (b) B. Y. Xia, Y. Yan, N. Li, H. B. Wu, X. W. Lou and X. Wang, *Nat. Energy*, 2016, **1**, 15006; (c) X. F. Hu, Z. Q. Zhu, F. Y. Chen, Z. L. Tao and J. Chen, *Nanoscale*, 2015, **7**, 11833; (d) W. Yin, W. Shen, F. Zou, X. Hu, B. Chi and Y. H. Huang, *ACS Appl. Mater. Interfaces*, 2015, **7**, 4947.
10 (a) X. Guo, B. Sun, J. Q. Zhang, H. Liu and G. X. Wang, *J. Mater. Chem. A*, 2016, **4**, 9774; (b) H. Y. Song, S. M. Xu, Y. J. Li, J. Q. Dai, A. Gong, M. W. Zhu, C. L. Zhu, C. J. Chen, Y. N. Chen, Y. G. Yao, B. Y. Liu, J. W. Song, G. Pastel and L. B. Hu, *Adv. Energy Mater.*, 2018, **8**, 1701203; (c) B. Sun, X. D. Huang, S. Q. Chen, P. Munroe and G. X. Wang, *Nano Lett.*, 2014, **14**, 3145; (d) J. Yi, S. C. Wu, S. Y. Bai, Y. Liu, N. Li and H. S. Zhou, *J. Mater. Chem. A*, 2016, **4**, 2403.
11 (a) F. F. Chao, B. X. Wang, J. J. Ren, Y. W. Lu, W. R. Zhang, X. Z. Wang, L. Cheng, Y. B. Lou and J. X. Chen, *J. Energy Chem.*, 2019, **35**, 212; (b) X. J. Wang, J. W. Zhou, H. Fu, W. Li, X. X. Fan, G. B. Xin, J. Zheng and X. G. Li, *J. Mater. Chem. A*, 2014, **2**, 14064; (c) S. J. You, X. B. Gong, W. Wang, D. P. Qi, X. H. Wang, X. D. Chen and N. Q. Ren, *Adv. Energy Mater.*, 2016, **6**, 1501497; (d) Z. H. Li, M. F. Shao, L. Zhou, R. K. Zhang, C. Zhang, M. Wei, D. G. Evans and X. Duan, *Adv. Mater.*, 2016, **28**, 2337; (e) F. L. Meng, H. X. Zhong, D. Bao, J. M. Yan and X. B. Zhang, *J. Am. Chem. Soc.*, 2016, **138**, 10226.
12 (a) Z. Y. Guo, F. M. Wang, Z. J. Li, Y. Yang, A. G. Tamirat, H. C. Qi, J. S. Han, W. Li, L. Wang and S. H. Feng, *J. Mater. Chem. A*, 2018, **6**, 22096; (b) S. X. Yang, Y. Qiao, P. He, Y. J. Liu, Z. Cheng, J. J. Zhu and H. S. Zhou, *Energy Environ. Sci.*, 2017, **10**, 972; (c) W. Xia, J. H. Zhu, W. H. Guo, L. An, D. G. Xia and R. Q. Zou, *J. Mater. Chem. A*, 2014, **2**, 11606; (d) A. Li, X. Zhang, Z. J. Xie, Z. Chang, Z. Zhou and X.-H. Bu, *Inorg. Chem.*, 2018, **57**, 14476; (e) A. Aijaz, J. Masa, C. Rösler, W. Xia, P. Weide, A. J. R. Botz, R. A. Fischer, W. Schuhmann and M. Muhler, *Angew. Chem., Int. Ed.*, 2016, **55**, 4087.